JPn Neuroscience

The Journal of Physiology

J Physiol 590.19 (2012) pp 4761–4775

Acid-sensing ion channels contribute to chemosensitivity of breathing-related neurons of the nucleus of the solitary tract

Rafiq Huda, Sarah L. Pollema-Mays, Zheng Chang, George F. Alheid, Donald R. McCrimmon and Marco Martina

Department of Physiology, Northwestern University Feinberg School of Medicine, 303 E Chicago Avenue, Chicago, IL 60611, USA

Key point

- A subset of neurons of the nucleus of the solitary tract (nucleus tractus solitarius, NTS) show a response to changes in pH within the physiological range (7.4 to 7.0) that is mediated by acid sensing ion channels (ASICs).
- These 'responder neurons' appear to cluster dorsally in the NTS.
- ASIC1 and ASIC2 transcripts are expressed in the NTS.
- NTS neurons projecting to the ventral respiratory column show ASIC-mediated responses to mild pH challenges and may modulate the respiratory response to P_{CO_2}.
- Injection of the ASIC inhibitor amiloride into the NTS transiently depresses breathing frequency in hypercapnic anaesthetized rats.

Abstract Cellular mechanisms of central pH chemosensitivity remain largely unknown. The nucleus of the solitary tract (NTS) integrates peripheral afferents with central pathways controlling breathing; NTS neurons function as central chemosensors, but only limited information exists concerning the ionic mechanisms involved. Acid-sensing ion channels (ASICs) mediate chemosensitivity in nociceptive terminals, where pH values ∼6.5 are not uncommon in inflammation, but are also abundantly expressed throughout the brain where pH is tightly regulated and their role is less clear. Here we test the hypothesis that ASICs are expressed in NTS neurons and contribute to intrinsic chemosensitivity and control of breathing. In electrophysiological recordings from acute rat NTS slices, ∼40% of NTS neurons responded to physiological acidification (pH 7.0) with a transient depolarization. This response was also present in dissociated neurons suggesting an intrinsic mechanism. In voltage clamp recordings in slices, a pH drop from 7.4 to 7.0 induced ASIC-like inward currents (blocked by 100 μM amiloride) in ∼40% of NTS neurons, while at pH $\leq$ 6.5 these currents were detected in all neurons tested; RT-PCR revealed expression of ASIC1 and, less abundantly, ASIC2 in the NTS. Anatomical analysis of dye-filled neurons showed that ASIC-dependent chemosensitive cells (cells responding to pH 7.0) cluster dorsally in the NTS. Using *in vivo* retrograde labelling from the ventral respiratory column, 90% (9/10) of the labelled neurons showed an ASIC-like response to pH 7.0, suggesting that ASIC currents contribute to control of breathing. Accordingly, amiloride injection into the NTS reduced phrenic nerve activity of anaesthetized rats with an elevated arterial P_{CO_2}.

(Received 16 March 2012; accepted after revision 8 August 2012; first published online 13 August 2012)
Corresponding author M. Martina: Department of Physiology, Northwestern University Feinberg School of Medicine, 303 E. Chicago Avenue, Chicago, IL 60611, USA. Email: m-martina@northwestern.edu

Abbreviations APV, 2-amino-5-phosphonopentanoic acid; ASIC, acid-sensing ion channel; CNQX, 6-cyano-7-nitroquinoxaline-2,3-dione; DLH, DL-homocysteate; NTS, nucleus of the solitary tract; VRC, ventral respiratory column.

DOI: 10.1113/jphysiol.2012.232470

Introduction

Central chemosensitivity plays an important role in cardiorespiratory homeostasis (Nattie, 2000). Chemosensitive responses have been recorded in several brain areas including the retrotrapezoid and preBötzinger nuclei of the ventrolateral medulla (Solomon, 2002; Guyenet, 2008), the medullary raphe (Severson *et al.* 2003), the locus coeruleus (Coates *et al.* 1993; Nichols *et al.* 2008), the hypothalamus (Dillon & Waldrop, 1993), the fastigial nucleus of the cerebellum (Xu *et al.* 2001) and the nucleus of the solitary tract (Dean *et al.* 1990; Coates *et al.* 1993; Nattie & Li, 2002, 2008), yet the precise mechanisms of central chemosensitivity remain unresolved. While the involvement of the nucleus of the solitary tract (nucleus tractus solitarius, NTS) in this function is strongly supported (Feldman *et al.* 2003; Dean & Putnam, 2010), the properties (location, size, electrophysiological phenotype) of the chemosensitive neurons within this nucleus are mostly unknown (Putnam *et al.* 2004). The relative impact of intrinsic neuronal mechanisms *versus* synaptic afferents in determining central chemoreception for various putative chemosensitive areas, and the nature of the ion channels mediating intrinsic chemosensitive responses also are still a matter of debate (Guyenet *et al.* 2010).

One straightforward mechanism for chemosensitivity is the direct activation of ion channels by a drop in extracellular pH levels. Although gating of many ion channels is modulated by large changes in extracellular proton concentration (Hille, 2001), only a small subset of ion channels are actually proton gated, that is channels that are modulated almost exclusively by extracellular pH variations and can respond to pH values within the physiological range of blood and cerebrospinal fluid (pH 6.8 to 7.8, Morgan *et al.* 2006). Such channels belong to four main families: TRPV, ASIC, KCNJ and KCNK. ASIC and TRPV channels open, while most KCNJ and KCNK channels close in response to extracellular acidification. pH-sensitive KCNK channels, such as TASK (Duprat *et al.* 1997), are nearly ubiquitous in the CNS where they are present in many different neuronal populations (Millar *et al.* 2000; Talley *et al.* 2001; Taverna *et al.* 2005). Consequently, it has been suggested that their expression is unlikely to define any specific cell type as a central chemosensor (Guyenet *et al.* 2008), although TASK1 plays a central role in peripheral chemosensitivity (Trapp *et al.* 2008). KCNJ channels seemed more promising, but a recent study showed that genetic ablation of Kir5.1 (KCNJ16) did not alter chemosensitivity. Hence, these channels are also unlikely to play a major role in functional central respiratory chemosensitivity (Trapp *et al.* 2011).

Acid-sensing ion channels (ASICs; Waldmann *et al.* 1997) are a subgroup of the degenerin/epithelial Na^+ channel family and are activated by low extracellular pH. This family has three genes (*Accn1–3*), all encoding channels that are mostly sodium selective, although other cations may permeate the channels with lower permeability (Bässler *et al.* 2001; Chen & Gründer, 2007). Interestingly, the half-activation proton concentration for some of these subunits is close to the physiological artificial cerebrospinal fluid (ACSF) range; $pH_{0.5}$ for ASIC1a is 6.6 (Hattori *et al.* 2009), and 6.7 for rat ASIC3 (Sutherland *et al.* 2001).

While the role of these channels in pain signalling in the PNS is well established, less is known about their potential role in the CNS, where they are robustly expressed and can mediate large currents (Pidoplichko & Dani, 2006; Weng *et al.* 2010). No report so far has described functional expression of ASIC currents in the medulla or their involvement in central chemoreception. Here we show that ASICs mediate chemosensitive responses in the rat NTS and that these responses are involved in control of breathing.

Methods

All animals were handled in accordance with National Institutes of Health and Northwestern University Animal Care and Use Committee guidelines.

Acute slice preparation

Coronal brainstem slices were obtained from 14- to 30-day-old Sprague–Dawley rats. Animals were deeply anaesthetized with isoflurane, and then decapitated. The brainstem was quickly removed into ice-cold low Ca^{2+}, high Mg^{2+} artificial cerebrospinal fluid (low Ca-ACSF, mM: 125 NaCl, 25 $NaHCO_3$, 2.5 KCl, 1.25 NaH_2PO_4, 25 glucose, 0.1 $CaCl_2$, and 7 $MgCl_2$) equilibrated with 95% O_2 and 5% CO_2.

Transverse slices of 275–300 μm containing the NTS (from ~800 μm caudal to obex to ~100 μm rostral to obex) were cut using a vibrating blade microtome (Thermo Scientific) and stored for ~30 min at 33–35°C, and at room temperature thereafter, in sucrose based ACSF (in mM: 87 NaCl, 25 $NaHCO_3$, 25 glucose, 75 sucrose, 2.5 KCl, 1.25 NaH_2PO_4, 0.5 $CaCl_2$, and 7 $MgCl_2$) equilibrated with 95% O_2 and 5% CO_2.

Slice recordings

Slices were transferred to a recording chamber constantly superfused with regular ACSF (in mM: 125 NaCl, 2.5 KCl, 25 $NaHCO_3$, 25 glucose, 1.8 $CaCl_2$, 1 $MgCl_2$) at 22–24°C. All slice experiments were conducted in the presence of 2.5 mM kynurenic acid, 100 μM picrotoxin, and 1 μM strychnine to block fast synaptic transmission. Recordings

were made with an Axopatch 200B (Molecular Devices, Sunnyvale, CA, USA) or MultiClamp 700A (Molecular Devices) amplifier, digitized with a 1440A Digidata acquisition board (Molecular Devices), and displayed and saved on a digital computer with Clampex 10.2 software (Molecular Devices). Slices were visualized with an upright microscope (Olympus) with oblique infrared illumination and videomicroscopy using a digital camera (DVC). Patch pipettes were fabricated from borosilicate capillary tubes (OD = 1.65 mm; ID = 0.75 mm, Dagan Corp., Minneapolis, MN, USA) using a horizontal puller (P97, Sutter Instrument Co., Novato, CA, USA) and had tip resistances of 2–5 MΩ when filled with working solution.

Current-clamp recordings were performed using a potassium gluconate-based solution (in mM: 130 potassium gluconate, 10 NaCl, 2 $MgCl_2$, 10 EGTA and 10 HEPES (pH 7.3 with KOH). A caesium-based intra-pipette solution was used for voltage clamp recordings and contained (in mM): 140 CsCl, 2 $MgCl_2$, 10 EGTA, 10 HEPES and 5 QX-314 (pH 7.3 with CsOH); 1 mg ml^{-1} lucifer yellow was also included in all recordings for *post hoc* identification and topographical analysis of the recorded neurons.

The extracellular solution was exchanged using focal pressure applications (10–20 psi) through puffer pipettes pulled from borosilicate theta glass tubing and connected to a Picospritzer II (General Valve Corp., East Hanover, NJ, USA). Low pH solutions were generated by titrating HEPES-ACSF with an appropriate quantity of NaOH. Similar to the bath solution, all puffer solutions also included blockers of fast synaptic transmission, although 10 μM 6-cyano-7-nitroquinoxaline-2,3-dione (CNQX) (in DMSO) and 50 μM D,L-APV (in H_2O) were used instead of kynurenic acid.

Drugs were dissolved in stock solutions (kynurenic acid, 500 mM in 1 N NaOH, picrotoxin 50 mM in DMSO, CNQX 10 mM in DMSO, D,L-APV 50 mM and strychnine 1 mM in H_2O) and stored at 2–3°C. Working solutions were prepared daily.

Dissociated cell preparation and electrophysiology

The procedure for obtaining dissociated NTS cells was adapted from Do & Bean (2004). Acute brainstem slices were visualized with a dissection microscope and the NTS was removed using a scalpel. NTS slices were incubated in dissociation solution (in mM: 70 Na_2SO_4, 1.5 K_2SO_4, 10 HEPES, 25 glucose, 75 sucrose, and 7 $MgCl_2$) containing 3 mg ml^{-1} protease XXIII for 5–7 min at 35°C. Slices were washed in the dissociation solution three times, then incubated in the presence of 1 mg ml^{-1} trypsin inhibitor and 3 mg ml^{-1} bovine serum albumin for ∼30 min at 21–23°C. Slices were stored in dissociation solution until they were mechanically dissociated using fire polished Pasteur pipettes of decreasing diameters. Dissociated cells were placed in a petri dish and allowed to settle for ∼15 min before washing in HEPES-buffered ACSF. The dish was placed on the stage of an inverted microscope (Nikon) for recordings and cells were visualized with a 20× objective. Whole-cell recordings were performed using an Axopatch 200B amplifier, digitized with Digidata 1200, and saved and displayed on a computer with Clampex 9.0. Current clamp and voltage clamp recordings were conducted with potassium gluconate and CsCl based internal solutions. Dissociated cells that retained some of their processes were selected for whole-cell recordings. In all cases, cells that met this criterion showed action potentials in response to positive current injections (or were spontaneously active), confirming their neuronal phenotype. Hence, for voltage clamp recordings that included QX-314 to block voltage gated Na^+ channels, this morphological feature was used to select neurons for recordings. Low pH solutions were locally applied to the cells by manually moving an array of quartz pipes (0.26 mm ID, 0.36 mm OD) with a micromanipulator. Solutions were gravity-fed to the pipes from reservoirs containing different pH solutions. A control solution (pH 7.4) was constantly applied through one of the pipes when the test solutions were not being applied.

Amiloride (100 μM) for both slice and dissociated cell experiments was prepared fresh from a 100 mM stock (in H_2O) on the day of the experiment.

Analysis of electrophysiological data

Electrophysiology data were analysed using Clampfit 10.2 software (Molecular Devices). For voltage clamp experiments, the amplitude of pH induced current was calculated by subtracting the baseline current in control solution from peak current in low pH solutions. For current clamp experiments in slices, a small negative current (5–30 pA) was injected to keep the resting potential around −70 mV and baseline voltage was subtracted from the peak voltage response to calculate the pH induced voltage change. For small responses, traces from up to five pH applications were averaged to calculate the peak response. In dissociated cells, pH responses were measured from resting potentials. In cases where neurons were spontaneously active, the average instantaneous discharge frequency at rest was compared with the average instantaneous discharge frequency during pH application. For neurons that responded transiently to pH 7.0, the average frequency was calculated at the peak of the response.

Comparisons between different cells were performed using Student's unpaired *t* test; Student's paired *t* test was used to compare the effect of a treatment on the same cell.

Two-tailed *t* tests were used, unless stated otherwise. All data are presented as means ± SEM. Error bars in graphs also represent ±SEM.

RT-PCR

The NTS was dissected from acute brainstem slices from two Sprague–Dawley rats. RNA from each NTS sample was independently purified using a High Pure RNA Isolation Kit (Roche, cat. no. 11828665001). Each sample was reverse transcribed using a First Strand cDNA Synthesis Kit (Roche, cat. no. 04897030001) using anchored oligo dT primers. cDNA was used for quantitative RT-PCR for ASIC1a, ASIC2 and ASIC3. The following primers were used: ASIC1a (GenBank accession no. NM_024154.2) forward primer: ATTCGAGACATGCTGCTCTC, reverse primer: CCTGACTGTGGATCTGCACT. ASIC2 (Gen Bank no. NM_012892.2) forward primer: TTACTT GGTGACATCGGTGG, reverse primer: TGTCTCCTGTC CTAGGTCTT. ASIC3 (GenBank no. NM_173135.1) forward primer: ATACCGCATCTTTGGATCCC, reverse primer: CTTGGCATAGCGTGTAGTAG). ASIC signals were normalized to glyceraldehyde-3-phosphate dehydrogenase (GAPDH; forward primer: CTGCACCACCAA CTGCTTAG, reverse primer: TGATGGCATGGACTGT GG). Quantitative RT-PCR was done using a Roche Light-Cylcer 480 with 20 μl Cyber Green reactions (cat. no. 04707516001). PCR consisted of a 6 min hot start at 95°C, followed by 45 cycles of 95°C for 30 s, 60°C for 20 s, and 30 s at 72°C. The two independent ASIC NTS samples were run in duplicate, normalized to GAPDH, and the relative abundance of ASIC1a *vs.* ASIC2 *vs.* ASIC3 calculated using Roche's Advanced Relative Quant delta-delta Ct method. All PCR data were efficiency corrected by generating standard curves for each primer set. PCR was also done using cDNA from the dorsal root ganglia as a positive control for ASIC transcript. The product sizes were 265, 323 and 287bp for ASIC1a, ASIC2 and ASIC3 respectively. Because no ASIC3 transcript was detected in the NTS, an additional primer pair for ASIC3 (forward primer: TGATGCATATGCCTGGAAAC, reverse primer: CAGACACACGTGTCCTTTCG) was generated and again no transcript was detected.

To ensure that genomic DNA did not contribute to the PCR products, ASIC primers were designed for intron-spanning regions. Additionally, control experiments were performed in which the reverse transcriptase was omitted.

Topographical analysis and two-dimensional model of the NTS

Slices containing cells filled with Lucifer yellow were fixed in phosphate buffered saline (PBS) containing 4% paraformaldehyde for 24–48 h, then stored in PBS for up to a week. 'Wet' sections were imaged with an epifluorescence microscope (Olympus) with a 5× or 10× objective (Olympus) to visualize the Lucifer yellow filled cells within the slice. Images were captured with a digital camera (QImaging Retiga 4000R) and data were analysed using ImageJ (NIH). The fluorescence image from each slice was combined with the bright-field trans-illuminated image of the same area placed in a separate colour channel. In order to plot cells from different slices obtained from different animals within the same Cartesian plot, we measured normalized X and Y values for each fluorescently labelled cell. The distance from the top of the central canal to the dorsal-most aspect of the NTS served as the maximal Y distance, whereas the distance from the midline to the centre of the solitary tract on either side served as the maximal $X(-)$ and $X(+)$ distances for a particular slice. Figure 6*A* shows how the values were practically calculated. The length of the vertical black continuous line labelled Y_{max} defines the Y-axis of the model coordinate system, and continuous lines labelled $X(-)_{max}$ and $X(+)_{max}$ define the X-axis of the model. The white dotted line labelled X_{cell} initiates from the centre of a cell, extends to the midline, and its length defines the X value for this cell. Similarly, the length of Y_{cell} line marks the distance of this cell from the top of the central canal (CC) and defines its Y value. The X_{cell} value was normalized by dividing it by the $X(-)_{max}$ or $X(+)_{max}$ value (depending on whether the cell was on the left or right side) and the Y_{cell} value was normalized by dividing it by the Y_{max} for each cell. These values were gathered for all recovered fluorescently labelled cells and plotted on the same Cartesian plot to obtain the graph in Fig. 6*B*.

The model was also used to calculate a proximity index (PI) for each neuron that responded to pH 7.0. First, the average distance between the kth responding neuron and all non-responders (R to NR), and all other responders (R to R) was determined using

$$\text{R to NR} = \frac{1}{m}\sum_{i=1}^{m}|Y_i - Y_k|$$

$$\text{R to R} = \frac{1}{n}\sum_{j=1}^{n}|Y_j - Y_k|$$

where Y_k is the normalized Y-axis distance from the origin of the kth responding neuron, m is the total number of non-responders, $\{Y_i, \ldots Y_m\}$ is the Y-axis distance for the non-responders, n is the total number of responders, and $\{Y_j, \ldots Y_n\}$ is the Y-axis distance for the responders. The PI was then calculated by using the formula PI = (R to NR) – (R to R). This formula calculates the difference between the average distance from a given responder to all non-responders and responders. Since there are only two responding neurons in the region corresponding to bin 5

in Fig. 6*C*, these cells were omitted from this analysis. The graph shown in Fig. 6*D* was generated by normalizing the PI values to the maximum PI obtained.

In vivo methods

Injection of retrograde tracers in juvenile rats. Sprague–Dawley rats (15–22 days old) of either sex were anaesthetized with isoflurane (5% induction, 2.5–3% maintenance). Adequacy of anaesthesia was evaluated at least every 15 min by assessing any withdrawal or changes in heart rate or respiration rate in response to a noxious paw pinch. Transcutaneous needle electrodes were placed over the caudal ribcage to record ECG and respiratory EMG as a marker of the inspiratory phase of breathing. Rectal temperature was monitored and maintained at 36.5–38.5°C by means of a thermistor-controlled heating pad and heat lamp. Oxygen saturation and heart rate were monitored throughout surgery via a pulse oximeter (Mouse Ox, Starr Life Sciences Oakmont, PA, USA).

Rats were placed in a stereotaxic headholder. A midline incision was made over the dorsal skull and a ∼2 × 2 mm window through the occipital plate was opened to expose the dorsal surface of the cerebellum. Extracellular unit activity was recorded (Fig. 1) to identify when the electrode was positioned within a cluster of respiratory neurons within the rostral ventral respiratory group in the ventrolateral medulla and a retrograde tracer was injected from adjacent barrels of a two-barrel glass pipette (theta tube) with aggregate external diameters ∼12–60 μm (∼6–30 μm per side). A recording barrel was filled with 150 mM NaCl, a 0.003″ silver wire inserted in the recording barrel, and the top end of the barrel sealed with an ∼2 mm long plug of fast setting UV-activated glue (Loctite 3492). The second barrel was filled with either a solution containing 20% rhodamine-impregnated latex beads (LumaFluor Inc., Durham, NC, USA) or 1% rhodamine-dextran amine (MW 3000, Invitrogen/Molecular Probes) suspended in 10 mM of the excitatory amino acid agonist DL-homocysteate (DLH). The electrode was then connected to a solenoid-valve controlled pressure injector via polyethylene tubing and sealed with UV curing glue. Pressure injections of small volumes of DLH into compartments of the ventral respiratory column (VRC) in the ventrolateral medulla elicit site-specific cardiorespiratory changes that, in combination with recording of respiratory units, identifies the specific compartment being injected (Monnier *et al.* 2003). Anterior portions of the VRC were targeted with initial recording/injection penetrations made at 3–4 mm caudal to the lambda suture and 1.5 mm lateral to the midline.

The pipette was advanced to the centre of the respiratory neuronal population (verified by recording spontaneous respiratory multi-unit activity; Fig. 1) and 30–45 nl of the rhodamine solution was incrementally injected at this site (Fig. 1, arrow). If respiratory activity was not observed, the electrode was withdrawn from the brainstem and moved 200 μm medial or lateral to the preceding electrode track and a second penetration initiated. Following the tracer injection, a minimum of 15 min was allowed prior to removal of the pipette to reduce the tendency to aspirate the tracer dorsally along the electrode tract. The non-steroidal anti-inflamatory drug meloxicam (1 mg kg^{-1}, S.C.) was then administered and the surgical wound sutured. Anaesthesia was discontinued and following recovery of the righting responses, the opiate analgesic buprenorphin was administered (0.03 mg kg^{-1}, S.C.). Buprenorphin was repeated 12 h post-operatively and meloxicam at 24 h. Following sufficient time for

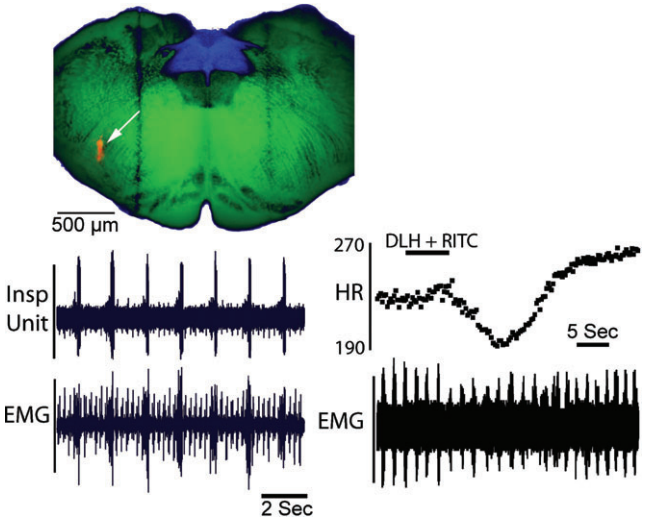

Figure 1. Electrophysiological recordings confirm the location for *in vivo* injection of retrograde tracers
Respiratory responses to a combined injection of rhodamine latex beads (RITC) and DL-homocysteate (DLH) into the rostral VRG. Upper left panel, transverse slice used for *in vitro* recording of NTS neurons and showing the injection site in the rVRG (arrow). Lower left panel, rVRG inspiratory unit activity (upper trace) recorded *in vivo* immediately prior to the RITC/DLH injection. Lower trace is respiratory muscle EMG and ECG recording. ECG potentials were graphically attenuated to enhance the respiratory EMG. Lower right panel, heart rate (upper trace, instantaneous frequency in beats min^{-1}) and respiratory EMG (lower trace) responses to a small injection (3 nl) of DLH and rhodamine latex beads as part of a total injection volume of 42 nl. Subsequent injection of a larger portion of the incremental injection produced a sustained apnoea and more marked bradycardia. The 300 μm thick medullary slice was captured as a brightfield image and light–dark inverted in Photoshop. Brightness and contrast for one copy of this image was adjusted to optimally show the myelinated fascicles in the green channel of a blank RGB image. A second copy was adjusted to optimize the NTS and was pasted in the blue channel of the RGB image. The epifluorescence image of the RITC injection was inserted into the red channel of the same RGB image. Dark vertical bands are the result of the nylon retaining bands in the *in vitro* chamber.

retrograde transport (at least 4 days) the animals were killed and used for *in vitro* recordings.

Assessing the effects of amiloride *in vivo*

Experiments were performed on three adult male Sprague–Dawley rats (vendor, Charles River) weighing 420–450 g. Rats were anaesthetized with isoflurane (5% induction, 2.5–3% maintenance). Adequacy of anaesthesia was assessed at least every 15 min noting any changes in heart rate, arterial pressure, or respiratory rate in response to a noxious paw pinch. A femoral vein and artery were catheterized for intravenous drug delivery and monitoring arterial pressure, respectively. Rats were tracheotomized, bilaterally vagotomized in the neck and mechanically ventilated with 50% O_2 (balance N_2) through a tracheal cannula (70 breaths min^{-1}; tidal volume 2.5–3 ml). End-tidal P_{CO_2} was continuously measured with an infrared analyser (Puritan-Bennett, Datex 223, Wilmington, MA, USA) modified to minimize dead space. End-tidal P_{CO_2} was adjusted by adding CO_2 to the inspired gas mixture. Rectal temperature was monitored and maintained between 37.5 and 38.5°C by means of a thermistor-controlled heating lamp.

Phrenic nerve recording. Rats were placed in a stereotaxic frame with the head ventroflexed such that the dorsal brainstem was approximately horizontal. A phrenic nerve was isolated using a dorsal approach in the neck, placed on a bipolar silver wire electrode and bathed in mineral oil for recording respiratory motor activity. Nerve activities were amplified, filtered (band pass 300 Hz to 10 kHz), full-wave rectified, and integrated (Paynter filter; time constant 15 ms). An occipital craniotomy was performed and the dura and arachnoid membranes removed to expose the dorsal surface of the brainstem at the level of the area postrema.

Amiloride injection. Glass micropipettes (1.2 mm OD, 0.68 mm ID) for drug delivery were pulled and broken to yield a tip with an outside diameter of 10–15 μm. The micropipettes were filled with amiloride (1 mM in 150 mM NaCl and a 10% solution of rhodamine-impregnated latex microspheres (for marking injection sites; Lumafluor Inc., Durham, NC, USA). For pressure injection, polyethylene tubing was sealed over the pipette end and connected to a regulated, solenoid valve-controlled pressure source. Injection volumes were directly monitored by measuring the movement of the fluid meniscus in the pipette using a compound microscope equipped with a fine reticule.

Experimental protocol. The pipette containing amiloride was positioned within the NTS 300–500 μm lateral to the midline, 300 μm rostral to 300 μm caudal to obex (the caudal tip of the area postrema), and 300–700 μm ventral to the dorsal surface. This area included the region containing significant numbers of chemosensitive neurons exhibiting ASIC-like conductances *in vitro*. Arterial P_{CO_2} was raised to 54–72 mmHg by increasing the fraction of inspired CO_2. At least 5 min was allowed for the respiratory motor output to stabilize and then amiloride was injected in relatively large volumes (50, 100 or 200 nl) to block ASIC activity in a relatively large region of the caudal NTS.

Histology. At the end of each experiment the animal was perfused transcardially under deep anaesthesia with 4% formaldehyde in 0.1 M phosphate buffer. The brainstem was removed and stored in the same fixative solution, but with 25% sucrose added. Coronal sections (50 or 75 μm) were cut on a vibrating blade microtome and the injection sites localized with a microscope and documented via digital photography.

Results

In order to study intrinsic chemosensitivity of NTS neurons, a first set of experiments was performed in acute slices. The recordings were made in the presence of picrotoxin (100 μM), strychnine (1 μM) and kynurenic acid (2.5 mM), to block $GABA_A$-, glycine- and glutamate-mediated transmission, respectively, and thus minimize the possible contribution of fast synaptic transmission to the chemosensitive response of individual NTS neurons.

Current clamp recordings were performed in the whole-cell configuration and extracellular pH was focally decreased by puffing HEPES-buffered ACSF titrated to pH 7.0 onto the patched cell (Fig. 2*A*). About 38% of cells (10 of 26) responded to this stimulus with a transient depolarization, ∼15% of cells (4 of 26) with a sustained depolarization, ∼27% hyperpolarized (7 of 26) and ∼19% (5 of 26) did not respond (Fig. 2*B*).

Because the data were obtained in the presence of fast synaptic transmission blockers they suggested that the observed pH-sensitive responses were mediated by intrinsic mechanisms. Nevertheless, a contribution of neurotransmitters, neuromodulators, or neuron–glia interaction to these responses could not be ruled out entirely. To study the intrinsic mechanisms in isolation, we performed whole-cell recordings on acutely dissociated NTS neurons. In these experiments, the extracellular solution consisted of HEPES-buffered ACSF, and extracellular acidification was obtained by lowering the extracellular pH from 7.4 to 7.0. The recordings from isolated NTS neurons showed that when the pH value dropped to 7.0, ∼33% (13 of 40) of the neurons responded with transient depolarizations,

30% (12/40) with sustained depolarization, 5% (2/40) hyperpolarized and ∼33% (13 of 40) did not show significant responses (Fig. 2*C* and *D*). A portion of the sustained depolarizing responses was accompanied by a decrease in the resting conductance (data not shown), likely to be due to inhibition of a potassium conductance as described previously (Dean *et al.* 1989). Thus, about two-thirds of acutely dissociated NTS neurons respond to pH with depolarizing responses, and more than half of these responses are transient, suggesting the possible involvement of ASICs.

Next, we performed voltage clamp recordings to better characterize the properties of the pH-dependent depolarizing current(s). We used a relatively large stimulus (pH 6.5, applied focally) to elicit large responses, which allow good signal to noise ratio, and to glean information about the kinetics and pharmacological profile of the conductance(s) involved. Cells responded to extracellular acidification with a depolarizing current that desensitized with a time constant (at −70 mV) of 2.01 ± 0.22 s, consistent with ASIC currents (Fig. 3). Therefore we tested the effects of amiloride (0.1 mM), a widely used ASIC blocker (Waldmann *et al.* 1997), on the pH-activated current. As shown in Fig. 3*A* and *B*, amiloride almost completely (86.6 ± 1.5%, $P < 0.05$, 5 cells) abolished the current, supporting the hypothesis that it was mediated by ASICs. These recordings suggest that ASICs are widely expressed in NTS neurons where they can be activated by extracellular pH ≤ 6.5. In keeping with this result, quantitative RT-PCR measurements detected abundant expression of ASIC1 and ASIC2 transcript in NTS tissue, with expression of ASIC1 about 10-fold that of ASIC2 (the ASIC/GAPDH ratio was 0.26 ± 0.01 for ASIC1 and 0.025 ± 0.013 for ASIC2; Fig. 3*C* and *D*).

While all NTS neurons responded to extracellular acidification to pH 6.5 with ASIC-like currents, only about 39% of NTS neurons showed intrinsic chemosensitivity to pH levels relevant for control of breathing (pH 7.0 to 7.4) in our experimental conditions. Thus, the next question was whether ASICs are also involved in the more physiologically relevant responses. To address this question, we reverted to the acute slice preparation to avoid possible artifacts induced in the current size and properties by the enzymatic treatment and subsequent mechanical dissociation (Poirot *et al.* 2004). Additionally, neurons recorded in NTS slices were loaded with intracellular dyes, allowing us to determine whether neurons excited by acidification show specific topographical organization within the NTS. Experiments were designed to investigate the amiloride sensitivity of the currents elicited by a physiological drop in the pH level (7.4 to 7.0) in slices. Again, amiloride (0.1 mM) strongly reduced the response (Fig. 4*A* and *B*) suggesting that it was largely mediated by ASICs. As expected, amiloride also effectively reduced

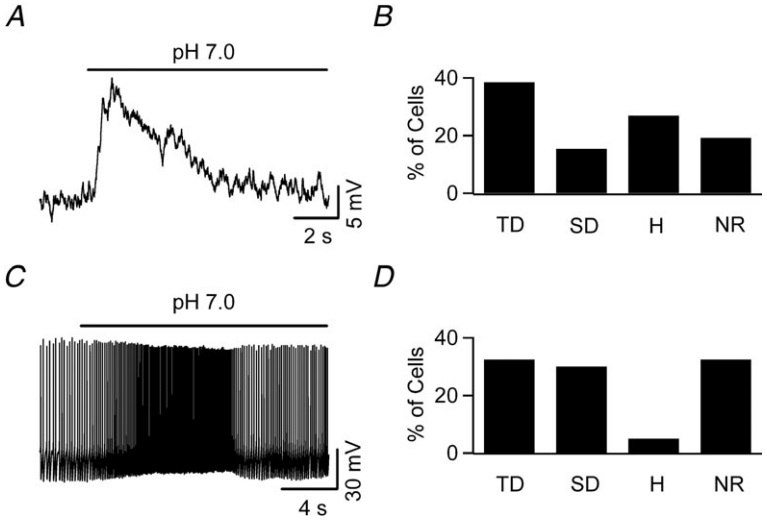

Figure 2. Heterogeneous responses of NTS neurons to mild extracellular acidification
A, focal application of a pH 7.0 solution transiently depolarized an NTS neuron in an acute brainstem slice. *B*, frequency profile of various responses elicited through mild extracellular acidification. Application of pH 7.0 onto NTS neurons ($n = 26$) in acute brainstem slices caused multiple types of response: transient depolarization (TD; 10 cells), sustained depolarization (SD; 4 cells), hyperpolarization (H; 7 cells), and no effect (NR; 5 cells). All slice experiments were conducted in the presence of blockers of fast synaptic neurotransmission (2.5 mM kynurenic acid, 100 μM Picrotoxin and 1 μM strychnine). *C*, whole-cell current clamp recording from an acutely dissociated NTS neuron shows a transient increase in the spontaneous discharge frequency during focal application of pH 7.0. *D*, focal acidification of the extracellular solution to pH 7.0 onto 40 acutely dissociated NTS neurons caused transient depolarization in 13 cells, sustained depolarization in 12 cells, hyperpolarization in 2 cells, and elicited no response from 13 cells.

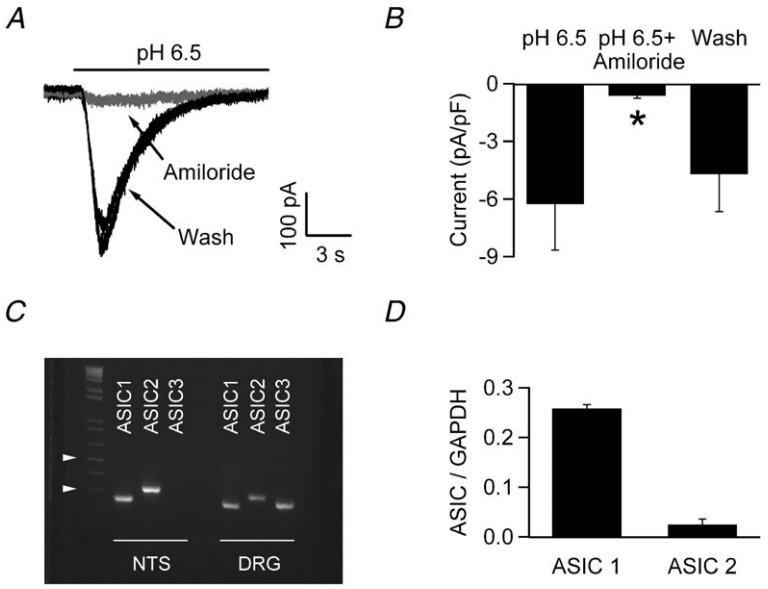

Figure 3. ASICs are widely expressed in NTS neurons
A, extracellular acidification to pH 6.5 elicits a desensitizing inward current from an acutely dissociated NTS neuron voltage clamped at −70 mV (black trace). Amiloride (100 μM, grey trace) reversibly blocks the pH induced current. *B*, bar chart showing the average effect of amiloride on pH 6.5 induced current (5 cells). *C*, ethidium bromide-stained gels of the PCR products amplified with primers specific for ASICs; ASIC1 and ASIC2 (but not ASIC3) transcripts were found in the NTS; control experiments on DRG tissue confirmed the efficiency of the ASIC3 primers. Arrowheads denote 500 and 300 bp, respectively. *D*, qPCR analysis using GAPDH as a reference gene showed that in the NTS ASIC1 is ∼10-fold more abundant than ASIC2.

the size of the transient depolarization induced by pH 7.0 (Fig. 4*C* and *D*). Notably, application of amiloride had no effect on sustained depolarizing responses to pH 7.0 (4.22 ± 1.73 *vs.* 4.17 ± 2.13 mV in pH 7.0 alone and co-applied with 0.1 mM amiloride, respectively; 3 cells), suggesting that these were mediated by a different mechanism. Similar to the current clamp data showing that only a fraction of NTS neurons exhibit ASIC-like responses to pH 7.0, in voltage-clamp not all the neurons responding to pH 6.5 also responded to pH 7.0. When pH 6.5 and 7.0 were tested on the very same neurons, all the cells examined responded to pH 6.5, but only ∼40% of them responded to pH 7.0 (Fig. 5*A*–*C*), a fraction similar to that (38%) showing a transient depolarization in response to extracellular acidification (Fig. 2).

These data show that ASIC currents are detectable in the rat NTS where they mediate a depolarizing response to physiologically relevant pH variations in ∼40% of cells, although all cells responded to larger pH drops. Next, we examined whether any difference in intrinsic electrophysiological properties such as cell size (capacitance) or input resistance could be detected between responders and non-responders. For this analysis cells that hyperpolarized in response to pH 7.0 were classified along with the non-responders, although they could play a role in chemosensitivity. No differences were detected in these parameters between responders and non-responders; the input resistance was 738 ± 80 and 803 ± 89 MΩ (45 and 53 cells) and the capacitance was 29.9 ± 1.8 and 30 ± 1.7 pF (51 and 69 cells, respectively).

While more work, including detailed kinetic and molecular analysis, may be required to pinpoint potential differences in the properties of ASIC currents in responders and non-responders, the existence of two distinct populations may be suggested if responders and non-responders are differentially localized within the

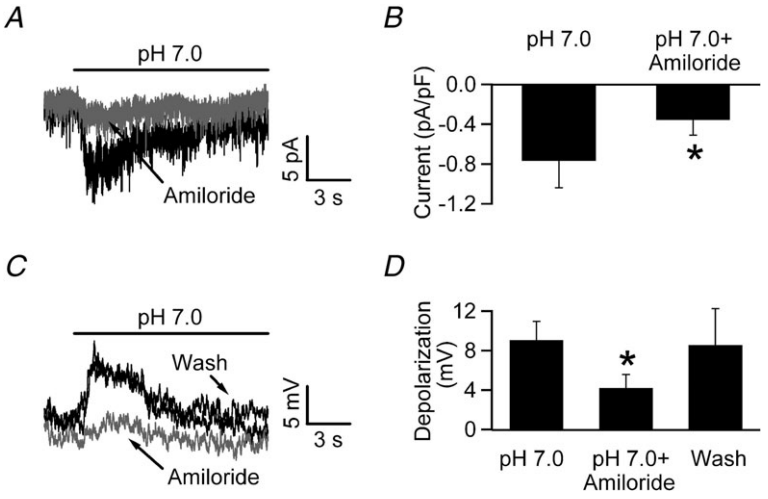

Figure 4. The currents evoked by pH 7.0 are amiloride sensitive
A, voltage clamp recording from an NTS neuron in acute slice. Focal application of pH 7.0 induced a desensitizing inward current that was substantially reduced by co-application of pH 7.0 and 100 μM amiloride. *B*, bar chart summarizing the results obtained in 3 different neurons. *C*, focal application of pH 7.0 in acute brain slices elicits a transient depolarization that is reversibly inhibited by 100 μM amiloride. *D*, bar chart depicting the net depolarization during focal application of pH 7.0 alone and in the presence of 100 μM amiloride (*$P < 0.05$; one-tailed Student's *t* test).

NTS. To test this hypothesis, a two-dimensional Cartesian model of the NTS was built and the localization of each recorded neuron was plotted in this space (Fig. 6*A* and *B*, see Methods). This analysis revealed that responder neurons tend to cluster in a relatively limited area of the NTS, with maximum likelihood in a region located between 333 and 445 μm dorsal from the top of the central canal (Fig. 6*B* and *C*). To further quantify this differential distribution, we computed and compared the average normalized Y distance from any particular responding neuron to all other responding neurons (R to R) and to all non-responding neurons (R to NR; see Methods). As expected, the average distance between responders located in this region to all other responders in the model was significantly smaller than the distance between responders and non-responders (0.208 ± 0.001 and 0.229 ± 0.001, respectively; $P < 0.05$). We also computed a proximity index (PI; see methods). This metric measures the difference between the R to NR and R to R distance. As shown in Fig. 6*D*, responder neurons located in the region have a positive PI value, indicating that they are, on average, closer to other responders than non-responders, confirming that responders are enriched in this region. Similarly, the current elicited by a pH drop from 7.4 to 7.0 was larger for cells in this area compared to other NTS regions (-17.5 ± 5.6 *vs.* -6.9 ± 1.2 pA, 7 and 8 cells, respectively, $P < 0.05$, one-tailed t test).

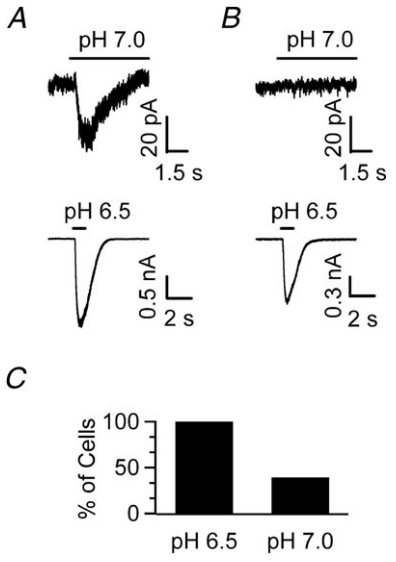

Figure 5. All NTS neurons express ASIC-like currents, but only a fraction respond to pH 7.0
A, voltage clamp recording obtained in an acute NTS slice from a neuron that responds to both pH 7.0 and pH 6.5 with a desensitizing, inward current. *B*, another NTS neuron shows an ASIC-like current to pH 6.5, but does not respond to pH 7.0. *C*, bar chart depicting the percentage of cells that respond to a stimulus of pH 6.5 or 7.0. While 100% of neurons respond to pH 6.5 (9/9), only 44.4% of neurons show an ASIC-like response to pH 7.0 (4/9).

Thus, a subset of NTS neurons preferentially located in the dorsal NTS (incorporating, but not restricted to, dorsal aspects of the commissural and medial nuclei) are capable of driving neuronal activity in response to small pH changes. Considering that the NTS is an important relay in the neuronal circuitry providing control of breathing, it is intriguing to suggest that these chemosensitive neurons project to the brainstem and spinal cord breathing-related cell groups and play a role in the central control of breathing. To investigate this hypothesis, fluorescent beads were injected into the principal group of bulbospinal inspiratory premotor neurons, the rostral ventral respiratory group (rVRG). This group receives a strong input from caudal NTS in the region that pH sensitive neurons were recorded (Alheid *et al.* 2011). Proper localization of the injection pipette within the rVRG was confirmed by recording respiratory neurons with the appropriate discharge pattern at the injection site in *in vivo* recordings from juvenile rats (Fig. 7*A*; see also Fig. 1); after 4–6 days the animals were killed and recordings were performed in acute NTS slices from neurons that contained the retrogradely transported beads (Fig. 7*B*). Intriguingly, while only ~40% of all NTS neurons are 'responders', 90% (9/10) of the retrogradely labelled neurons showed ASIC-like responses to pH 7.0 (Fig. 7*C* and *D*), suggesting that the ASIC current of these NTS neurons mediates a chemosensitive response that is involved in control of breathing. These data suggest that blocking ASIC currents in the NTS would reduce the respiratory motor output during hypercapnia. This hypothesis was tested directly by recording the phrenic nerve activity during hypercapnia in anaesthetized rats in control conditions and in the presence of focal application of the ASIC blocker amiloride in the NTS.

The burst frequency and peak amplitude of phrenic nerve bursts were measured during respiratory acidosis produced by increasing the inspired fractional concentration delivered via the ventilator (P_{CO_2} 54–72 mmHg, $n = 3$). As expected, respiratory acidosis strongly increased phrenic motor discharge (not shown); subsequent focal application of amiloride (50–200 nl; 1 mM) strongly and transiently reduced the burst frequency of the phrenic nerve (Fig. 8), consistent with the hypothesis that ASIC currents in the NTS are involved in the homeostatic control of breathing. There was also a moderate decrease in arterial pressure in the experiment shown in Fig. 8*A*, but this was not a consistent finding across all animals (Fig. 8*B*).

Discussion

Electrophysiological recordings were performed to investigate the intrinsic chemosensitive responses of

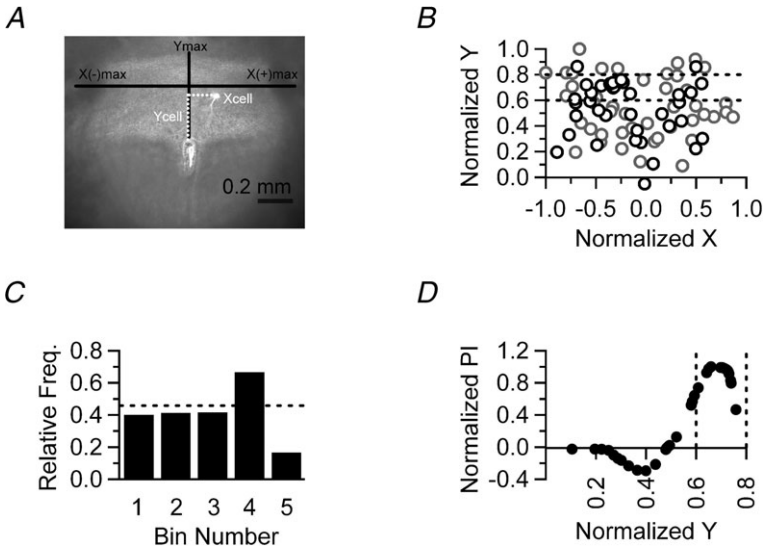

Figure 6. Topographical mapping of NTS neurons showing ASIC-like response to pH 7.0
A, representative photomicrograph of a brainstem slice used to create a two dimensional, Cartesian representation of the NTS (see Methods). *B*, normalized positions of 86 NTS neurons from 37 brainstem slices acquired from 21 animals plotted in a Cartesian model of the NTS. Neurons that responded to pH 7.0 are plotted as black circles, whereas non-responders are plotted as grey circles. Dotted lines demarcate a region of the model NTS (bin 4 in *C*) which contains the highest percentage of responding neurons. *C*, the *Y*-axis was divided into 5 bins of 0.2 arbitrary units (normalized *Y* distance). The histogram depicts the relative frequency of cells that respond to pH 7.0 within each bin. The dotted line indicates the overall probability of finding a neuron that responds to pH 7.0. Neurons that respond to pH 7.0 are enriched in bin 4. *D*, the *Y*-axis location of responders (from *B*) is plotted against their normalized proximity index (see Methods). Note that a positive value indicates that a cell is, on average, closer to other responders. Dotted vertical lines denote bin 4 (as in *B* and *C*).

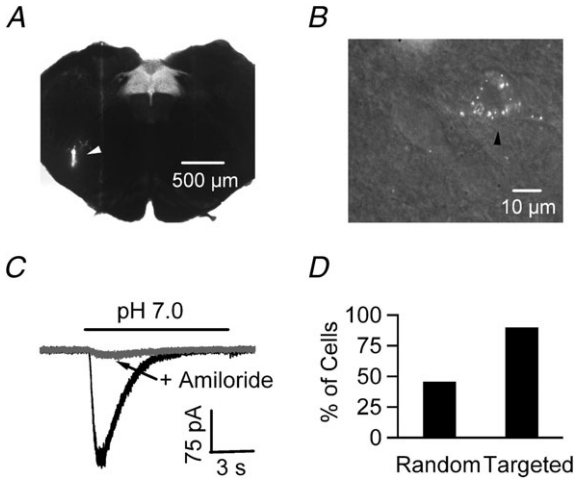

Figure 7. VRC-projecting NTS neurons show ASIC-like depolarization in response to pH 7.0
A, photomicrograph of a brainstem slice containing the NTS. The white arrowhead points to the site where retrograde beads were injected in the ventral respiratory column (VRC) *in vivo*. *B*, 60× magnification image of a brainstem slice from the same animal as in *A*. The black arrowhead shows a NTS neuron containing the retrogradely transported beads that was targeted for a current clamp patch recording. *C*, focal acidification to pH 7.0 of a labelled neuron reveals a transient current that is inhibited by 100 μM amiloride. *D*, while ∼40% of cells show ASIC-like responses to pH 7.0 using random patching, 90% (9/10) of VRC-projecting NTS neurons are responsive.

NTS neurons. Previous studies identified a significant population of neurons within the NTS that respond to local acidification or increases in P_{CO_2} (for reviews see Putnam *et al.* 2004; Dean & Putnam, 2010). Huang *et al.* (1997), for example, noted that ∼34% of the medium to large sized dorsal medullary neurons in tissue slices were excited by acidification within the normal physiological pH range. Inhibition of synaptic transmission with high Mg^{2+}–low Ca^{2+} reduced this proportion to about 24%. Although the high Mg^{2+}–low Ca^{2+} approach is unlikely to completely block all synaptic transmission, the observation that, in our study, ∼60% of acutely dissociated NTS neurons were excited by mild pH drop strongly supports the hypothesis that intrinsic mechanisms are instrumental to the chemosensitivity of NTS neurons (Dean *et al.* 1990, Huang *et al.* 1997).

Previous studies have shown that acidification can excite NTS neurons by inhibiting a K^+ conductance (Dean *et al.* 1989). Our voltage clamp recordings were made with a caesium-based internal solution, thereby minimizing the contribution of this mechanism to the observed responses to pH 7.0; however, our current clamp recordings (performed with potassium gluconate-based internal solution) suggest that a subset of the sustained depolarizing responses are insensitive to amiloride and are likely to be due to down-modulation of a potassium conductance, confirming this previous

finding. In addition, we found that a large subset of NTS cells responded to mild extracellular acidification with a transient depolarization that could be attributed to the activation of an ASIC current. We also show that while only ~40% of NTS neurons show ASIC-like responses to pH 7.0, this fraction is enriched within the more dorsal regions of the NTS, where up to 2 in 3 cells show this type of response.

ASICs are expressed in the NTS

All the NTS neurons tested showed an ASIC-like response when challenged with extracellular pH 6.5, although only ~40% of neurons were capable of depolarizing in response to pH 7.0. It is conceivable that this result may, in part, be the consequence of experimental artifacts; indeed, in the slice it is almost impossible to obtain complete exchange of the extracellular solution in less than a few hundred milliseconds, and so subthreshold desensitization could affect the responses. In keeping with this possibility, no differences were found in the basic electrophysiological properties of responders and non-responders. Yet, the anatomical data show that the responder neurons are preferentially distributed in the dorsal regions of the NTS, suggesting the existence in the NTS of two different classes of neurons; the fact that retrogradely labelled neurons in the breathing pathway responded to mild acidification more often than randomly recorded NTS neurons further supports the hypothesis of two different populations. If we

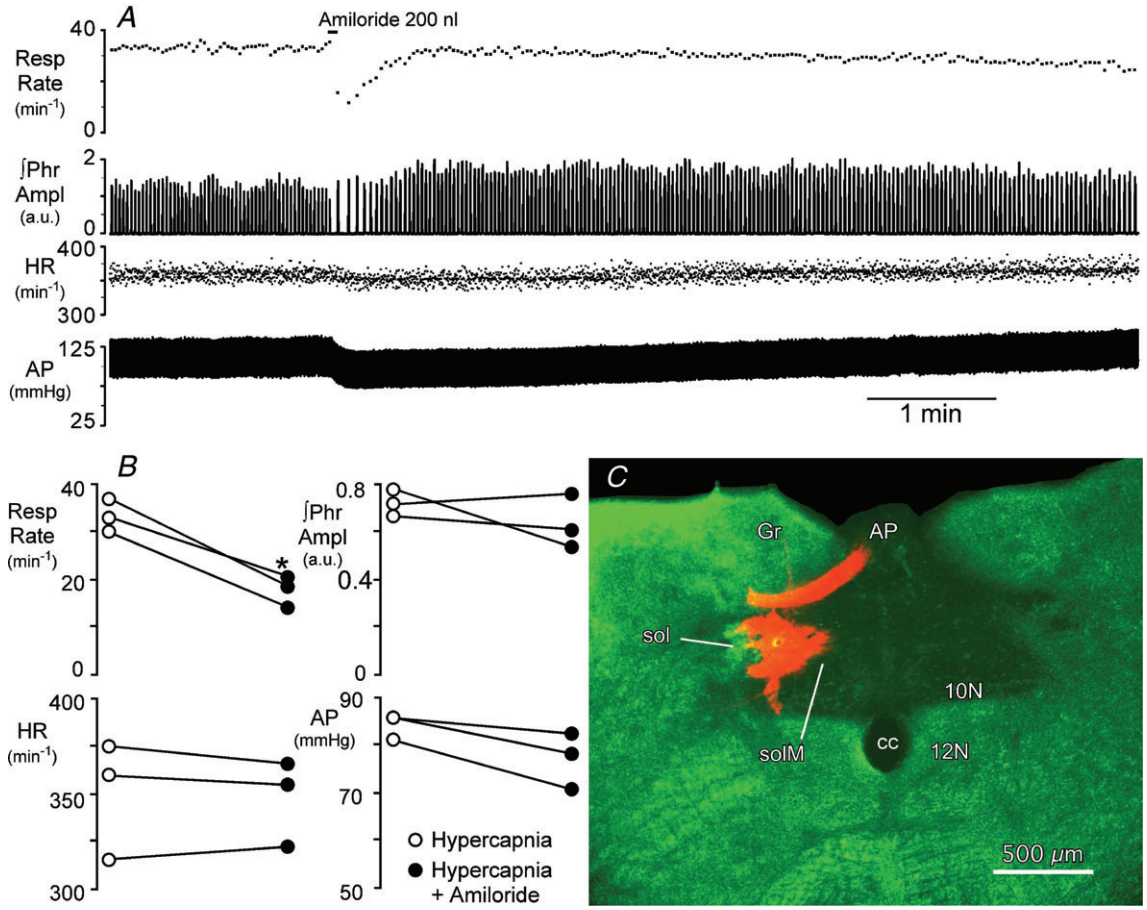

Figure 8. Blockade of ASIC current within the caudal NTS reduces respiratory motor output during hypercapnia (end-tidal P_{CO_2} = 54 mmHg)
A, injection of amiloride (2×10^{-10} mol in 200 nl) centred in the medial NTS (SolM) 300 μm rostral to obex, transiently reduces phrenic nerve burst frequency (Resp Rate) and arterial pressure (AP) but has little effect on the peak amplitude of integrated phrenic nerve activity (∫Phr) or heart rate (HR). *B*, peak changes in cardiorespiratory variables during injection of amiloride compared to hypercapnic control. *Significant decrease in respiratory rate *vs.* control ($P < 0.05$). *C*, coronal, pseudocoloured image of the injection site in SolM for the rat shown in *A*. Monochrome image of the rhodamine impregnated microspheres (red) and the darkfield image (green) were inserted into the red and green channels of a digital image. 10N, dorsal motor nucleus of the vagus; 12N, hypoglossal nucleus; AP, area postrema; cc, central canal; Gr, gracile nucleus; sol, solitary tract.

accept the idea of two distinct neuronal populations, we expect that some differences in the molecular composition of the channels will be measureable. RT-PCR analysis of NTS tissue detected abundant expression of ASIC1 and, to a lesser extent, ASIC2 transcript. Because our data show that all NTS neurons are endowed with ASIC currents but only a fraction are responders, it may be hypothesized that ASIC2, the less abundant subunit, is important for the response to mild acidification in these cells. This interpretation would match the observation that transgenic mice lacking expression of the ASIC1a subunit do not show any obvious defect in the ventilatory response to CO_2 inhalation (Ziemann *et al.* 2009). ASIC2 homomeric channels, on the other hand, require larger acidifications to activate (Benson *et al.* 2002; Hesselager *et al.* 2004; Hattori *et al.* 2009) compared to ASIC1a homomeric channels, which were shown to effectively respond to pH 7.2 in amygdala neurons (Ziemann *et al.* 2009). However, since native ASICs are often heteromeric (Benson *et al.* 2002; Baron *et al.* 2008; Hattori *et al.* 2009), it may be suggested that ASIC2 subunits in NTS cells may be present in heteromeric channels only, an interpretation in line with the finding that ASIC2b subunits coexpressed with ASIC1a in *Xenopus* oocytes form heteromeric channels with pH sensitivity similar to that of ASIC1a homomeric channels (Sherwood *et al.* 2011). A problem with this hypothesis is represented by the fact that ASIC2 channels could not be effectively activated at $pH > 5$ in hippocampal neurons from ASIC1–/– mice (Askwith *et al.* 2004). These data, however, were obtained on cultured neurons in which tissue-dependent metabolic modulation of ASICs is missing. Such a modulation plays a critical role in setting the pH sensitivity of ASICs; for example, the nitric oxide donor SNAP potentiates the response of ASIC2a to relatively mild pH (pH 6.3) by more than 250% (Cadiou *et al.* 2007). Additionally, if ASICs are indeed important for breathing, it must be expected that compensatory mechanisms, which are common in knockout animals, are more effective in the NTS than in the hippocampus. Thus, the precise role of ASIC2 subunits in the NTS remains unclear. ASIC3 transcript was not detected in the NTS; this was somewhat surprising because ASIC3 seemed potentially relevant for intrinsic chemosensitivity as these subunits generate a current that activates at less acidic pH and have large sustained components (Sutherland *et al.* 2001; Hesselager *et al.* 2004). However, it is worth stressing that the amplitude of the sustained fraction of ASIC currents appears to undergo regulation by neuromdulators such as peptides FF and SF (Deval *et al.* 2003) thus suggesting that in the brain the fraction of sustained current may be largely different from that in acute slices. More work will be required to investigate the subunit expression of ASIC subunits in different functional classes of NTS neurons.

ASIC-mediated chemosensitivity and control of breathing

A fraction of NTS neurons are endowed with ASIC currents that activate in response to even mild acidification (pH7.4 to 7.0); interestingly, the density of such neurons appears enriched in the dorsal NTS suggesting that ASIC-mediated pH responses may form selective synaptic contacts and have a well defined functional role. The observation that the ASIC-mediated current is found in NTS neurons retrogradely labelled from the VRC further suggests that this role is linked to cardiorespiratory control. The potential impact on a highly integrated *in vivo* function such as control of breathing, however, may be difficult to extrapolate from *in vitro* data also because brainstem neuron excitability has been shown to be affected by the hyperoxic condition typical of *in vitro* recordings (Mulkey *et al.* 2003; Dean *et al.* 2004). Therefore, *in vivo* experiments were performed to investigate the potential role of NTS ASIC conductance in the control of breathing during the condition of elevated arterial P_{CO_2} (∼70 mmHg). The *in vivo* measurements showed that infusion of amiloride in the NTS significantly reduced the phrenic nerve burst frequency in hypercapnic conditions. While this observation is in line with a potential role of ASICs in the control of breathing, it must be kept in mind that, beside ASICs, amiloride inhibits other channels (such as T-type calcium channels; Tang *et al.* 1988) and transporters (such as the Na^+/H^+ exchanger in NTS neurons; Ritucci *et al.* 1997). However, if the effect on the exchanger were predominant it might be expected to enhance rather than reduce breathing frequency, and thus such an effect appears unlikely. Nevertheless, our data must be interpreted cautiously and further investigations are needed to clarify the precise mechanisms of the amiloride effect on control of breathing. In particular, future experiments in which the effect of amiloride is compared in normocapnic and hypercapnic conditions will be required to support the specificity of the observed effects. We obtained preliminary data (not shown) suggesting that the effect of amiloride is indeed stronger in hypercapnic than in normocapnic conditions, but much more extensive studies will be necessary to properly address this important point. Moreover, the largely transient nature of the ASIC-mediated response may not appear ideally suited to mediate slow and long-lasting responses such as those required to produce the sustained changes in breathing in response to an acid–base disorder that may continue for months or years. This apparent clash between the gating properties of ASICs and their possible functional role is reminiscent of the role of ASICs in the pain response to nociceptive acidosis (such as in cardiac ischaemic pain). The same ASICs found in NTS neurons are suggested to mediate ischaemic pain (Hattori *et al.*

2009), which can last for hours or days. Several possible mechanisms could explain a role for transient currents in a slow and long-lasting process as control of breathing. A potential explanation may simply lay in the kinetic properties of ASIC2 containing channels, which are considerably slower than other ASICs (Waldmann *et al.* 1997; Staruschenko *et al.* 2007; Hattori *et al.* 2009). In keeping with this hypothesis we found neurons in which the pH-induced response was slowly decaying and showed a steady-state component (not shown), although different ion channels could also contribute to these responses. Another possibility resides in the large number of molecules, ranging from CamKII to metals like zinc (Baron *et al.* 2001) and nickel (Staruschenko *et al.* 2007) that can interact with ASICs and modify their pH sensitivity and kinetics (Wemmie *et al.* 2006). It is possible that interactions between such molecules and ASICs *in vivo* enhance the sustained component of the ASIC response. The recent intriguing discovery of a close molecular interaction between ASIC3 and P2X receptors, which leads to substantial sensitization of the ASIC current (Birdsong *et al.* 2010), further strengthens this possibility. Finally, it may be suggested that the ASIC current only acts as the trigger for a response that is maintained by other mechanisms. In such a framework, the proton permeability of ASICs (Chen & Gründer, 2007) may play an important role as it has been suggested that the intracellular pH value provides an important signal in central chemoreception while changes of extracellular pH mostly modulate intracellular pH changes (Ritucci *et al.* 1998).

It is also worth noting that the responder neurons cluster in the dorsal NTS. Because this area is an important target for peripheral afferents from the lungs and airways (Kubin *et al.* 2006), it could be suggested that the chemosensitive neurons may represent second order neurons that integrate peripheral inputs and central acid–base status. As such, chemosensitive NTS neurons may play an important role in modulating cardiorespiratory or even gastrointestinal reflexes. It is known, for example, that the Breuer–Hering respiratory reflexes, mediated by afferents that terminate in the NTS, are strongly modulated by changes in pH (Mitchell & Vidruk 1987). Interestingly, pH may also modulate neurotransmitter release at the NTS synapses, as it is partly mediated by TRPV1 channels (Peters *et al.* 2010), which are modulated by extracellular protons (Caterina *et al.* 1997; Tominaga *et al.* 1998). Such a model in which multiple intrinsic and synaptic mechanisms necessarily interact in response to pH variations fits well with the idea of an extremely complex network in which each mechanism may be necessary but by itself not sufficient to produce the phenotype.

References

Alheid GF, Jiao W & McCrimmon DR (2011). Caudal nuclei of the rat nucleus of the solitary tract differentially innervate respiratory compartments within the ventrolateral medulla. *Neuroscience* **190**, 207–227.

Askwith CC, Wemmie JA, Price MP, Rokhlina T & Welsh MJ (2004). Acid-sensing ion channel 2 (ASIC2) modulates ASIC1 H^+-activated currents in hippocampal neurons. *J Biol Chem* **279**, 18296–18305.

Baron A, Schaefer L, Lingueglia E, Champigny G & Lazdunski M (2001). Zn^{2+} and H^+ are coactivators of acid-sensing ion channels. *J Biol Chem* **276**, 35361–35367.

Baron A, Voilley N, Lazdunski M & Lingueglia E (2008). Acid sensing ion channels in dorsal spinal cord neurons. *J Neurosci* **28**, 1498–1508.

Bässler EL, Ngo-Anh TJ, Geisler HS, Ruppersberg JP & Gründer S (2001). Molecular and functional characterization of acid-sensing ion channel (ASIC) 1b. *J Biol Chem* **276**, 33782–33787.

Benson CJ, Xie J, Wemmie JA, Price MP, Henss JM, Welsh MJ & Snyder PM (2002). Heteromultimers of DEG/ENaC subunits form H^+-gated channels in mouse sensory neurons. *Proc Natl Acad Sci U S A* **99**, 2338–2343.

Birdsong WT, Fierro L, Williams FG, Spelta V, Naves LA, Knowles M, Marsh-Haffner J, Adelman JP, Almers W, Elde RP & McCleskey EW (2010). Sensing muscle ischemia: coincident detection of acid and ATP via interplay of two ion channels. *Neuron* **68**, 739–749.

Cadiou H, Studer M, Jones NG, Smith ES, Ballard A, McMahon SB & McNaughton PA (2007). Modulation of acid-sensing ion channel activity by nitric oxide. *J Neurosci* **27**, 13251–13260.

Caterina MJ, Schumacher MA, Tominaga M, Rosen TA, Levine JD & Julius D (1997). The capsaicin receptor: a heat-activated ion channel in the pain pathway. *Nature* **389**, 816–824.

Chen X & Gründer S (2007). Permeating protons contribute to tachyphylaxis of the acid-sensing ion channel (ASIC) 1a. *J Physiol* **579**, 657–670.

Coates EL, Li A & Nattie EE (1993). Widespread sites of brain stem ventilatory chemoreceptors. *J Appl Physiol* **75**, 5–14.

Dean JB, Bayliss DA, Erickson JT, Lawing WL & Millhorn DE (1990). Depolarization and stimulation of neurons in nucleus tractus solitarii by carbon dioxide does not require chemical synaptic input. *Neurosci* **36**, 207–216.

Dean JB, Lawing WL & Millhorn DE (1989). CO_2 decreases membrane conductance and depolarizes neurons in the nucleus tractus solitarii. *Exp Brain Res* **76**, 656–661.

Dean JB, Mulkey DK, Henderson RA 3rd, Potter SJ & Putnam RW (2004). Hyperoxia, reactive oxygen species, and hyperventilation: oxygen sensitivity of brain stem neurons. *J Appl Physiol* **96**, 784–791.

Dean JB & Putnam RW (2010). The caudal solitary complex is a site of central CO_2 chemoreception and integration of multiple systems that regulate expired CO_2. *Respir Physiol Neurobiol* **173**, 274–287.

Deval E, Baron A, Lingueglia E, Mazarguil H, Zajac JM & Lazdunski M (2003). Effects of neuropeptide SF and related peptides on acid sensing ion channel 3 and sensory neuron excitability. *Neuropharmacology* **44**, 662–671.

Dillon GH & Waldrop TG (1993). Responses of feline caudal hypothalamic cardiorespiratory neurons to hypoxia and hypercapnia. *Exp Brain Res* **96**, 260–272.

Do MT & Bean BP (2004). Sodium currents in subthalamic nucleus neurons from Nav1.6-null mice. *J Neurophysiol* **92**, 726–733.

Duprat F, Lesage F, Fink M, Reyes R, Heurteaux C & Lazdunski M (1997). TASK, a human background K^+ channel to sense external pH variations near physiological pH. *EMBO J* **16**, 5464–5471.

Feldman JL, Mitchell GS & Nattie EE (2003). Breathing: Rhythmicity, plasticity, chemosensitivity. *Annu Rev Neurosci* **26**, 239–266.

Guyenet PG (2008). The 2008 Carl Ludwig Lecture: retrotrapezoid nucleus, CO_2 homeostasis, and breathing automaticity. *J Appl Physiol* **105**, 404–416.

Guyenet PG, Stornetta RL & Bayliss DA (2008). Retrotrapezoid nucleus and central chemoreception. *J Physiol* **586**, 2043–2048.

Guyenet PG, Stornetta RL & Bayliss DA (2010). Central respiratory chemoreception. *J Comp Neurol* **518**, 3883–3906.

Hattori T, Chen J, Harding AM, Price MP, Lu Y, Abboud FM & Benson CJ (2009). ASIC2a and ASIC3 heteromultimerize to form pH-sensitive channels in mouse cardiac dorsal root ganglia neurons. *Circ Res* **105**, 279–286.

Hesselager M, Timmermann DB & Ahring PK (2004). pH dependency and desensitization kinetics of heterologously expressed combinations of acid-sensing ion channel subunits. *J Biol Chem* **279**, 11006–11015.

Hille B (2001). *Ionic Channels of Excitable Membranes*. Sinauer Associates Inc., Sunderland, MA.

Huang RQ, Erlichman JS & Dean JB (1997). Cell-cell coupling between CO_2-excited neurons in the dorsal medulla oblongata. *Neuroscience* **80**, 41–57.

Kubin L, Alheid GF, Zuperku EJ & McCrimmon DR (2006). Central pathways of pulmonary and lower airway vagal afferents. *J Appl Physiol* **101**, 618–627.

Millar JA, Barratt L, Southan AP, Page KM, Fyffe RE, Robertson B & Mathie A (2000). A functional role for the two-pore domain potassium channel TASK-1 in cerebellar granule neurons. *Proc Natl Acad Sci U S A* **97**, 3614–3618.

Mitchell GS & Vidruk EH (1987). Effects of hypercapnia on phrenic and stretch receptor responses to lung inflation. *Respir Physiol* **68**, 319–330.

Monnier A, Alheid GF & McCrimmon DR (2003). Defining ventral medullary respiratory compartments with a glutamate receptor agonist in the rat. *J Physiol* **548**, 859–874.

Morgan GE Jr, Mikhail MS & Murray, MJ (2006). *Clinical Anesthesiology*, 4th edition. McGraw-Hill Companies, Inc. New York, NY, USA.

Mulkey DK, Henderson RA 3rd, Putnam RW & Dean JB (2003). Hyperbaric oxygen and chemical oxidants stimulate CO2/H^+-sensitive neurons in rat brain stem slices. *J Appl Physiol* **95**, 910–921.

Nattie E (2000). Multiple sites for central chemoreception: their roles in response sensitivity and in sleep and wakefulness. *Respir Physiol* **122**, 223–235.

Nattie E & Li A (2002). CO_2 dialysis in nucleus tractus solitarius region of rat increases ventilation in sleep and wakefulness. *J Appl Physiol* **92**, 2119–2130.

Nattie E & Li A (2008). Muscimol dialysis into the caudal aspect of the nucleus tractus solitarii of conscious rats inhibits chemoreception. *Respir Physiol Neurobiol* **164**, 394–400.

Nichols NL, Hartzler LK, Conrad SC, Dean JB & Putnam RW (2008). Intrinsic chemosensitivity of individual nucleus tractus solitarius (NTS) and locus coeruleus (LC) neurons from neonatal rats. *Adv Exp Med Biol* **605**, 348–352.

Peters JH, McDougall SJ, Fawley JA, Smith SM & Andresen MC (2010). Primary afferent activation of thermosensitive TRPV1 triggers asynchronous glutamate release at central neurons. *Neuron* **65**, 657–669.

Pidoplichko VI & Dani JA (2006). Acid-sensitive ionic channels in midbrain dopamine neurons are sensitive to ammonium, which may contribute to hyperammonemia damage. *Proc Natl Acad Sci U S A* **103**, 11376–11380.

Poirot O, Vukicevic M, Boesch A & Kellenberger S (2004). Selective regulation of acid-sensing ion channel 1 by serine proteases. *J Biol Chem* **279**, 38448–38457.

Putnam RW, Filosa JA & Ritucci NA (2004). Cellular mechanisms involved in CO_2 and acid signaling in chemosensitive neurons. *Am J Physiol Cell Physiol* **287**, C1493–C1526.

Ritucci NA, Chambers-Kersh L, Dean JB & Putnam RW (1998). Intracellular pH regulation in neurons from chemosensitive and nonchemosensitive areas of the medulla. *Am J Physiol Regul Integr Comp Physiol* **275**, R1152–R1163.

Ritucci NA, Dean JB & Putnam RW (1997). Intracellular pH response to hypercapnia in neurons from chemosensitive areas of the medulla. *Am J Physiol Regul Integr Comp Physiol* **273**, R433–R441.

Severson CA, Wang W, Pieribone VA, Dohle CI & Richerson GB (2003). Midbrain serotonergic neurons are central pH chemoreceptors. *Nat Neurosci* **6**, 1139–1140.

Sherwood TW, Lee KG, Gormley MG & Askwith CC (2011). Heteromeric acid-sensing ion channels (ASICs) composed of ASIC2b and ASIC1a display novel channel properties and contribute to acidosis-induced neuronal death. *J Neurosci* **31**, 9723–9734.

Solomon IC (2002). Modulation of expiratory motor output evoked by chemical activation of pre-Bötzinger complex in vivo. *Respir Physiol Neurobiol* **130**, 235–251.

Staruschenko A, Dorofeeva NA, Bolshakov KV & Stockand JD (2007). Subunit-dependent cadmium and nickel inhibition of acid-sensing ion channels. *Dev Neurobiol* **67**, 97–107.

Sutherland SP, Benson CJ, Adelman JP & McCleskey EW (2001). Acid-sensing ion channel 3 matches the acid-gated current in cardiac ischemia-sensing neurons. *Proc Natl Acad Sci U S A* **98**, 711–716.

Talley EM, Solórzano G, Lei Q, Kim D & Bayliss DA (2001). CNS distribution of members of the two-pore-domain (KCNK) potassium channel family. *J Neurosci* **21**, 7491–7505.

Tang CM, Presser F & Morad M (1988). Amiloride selectively blocks the low threshold (T) calcium channel. *Science* **240**, 213–215.

Taverna S, Tkatch T, Metz AE, Martina M (2005). Differential expression of TASK channels between horizontal interneurons and pyramidal cells of rat hippocampus. *J Neurosci* **25**, 9162–9170.

Tominaga M, Caterina MJ, Malmberg AB, Rosen TA, Gilbert H, Skinner K, Raumann BE, Basbaum AI, Julius D (1998). The cloned capsaicin receptor integrates multiple pain-producing stimuli. *Neuron* **21**, 531–543.

Trapp S, Aller MI, Wisden W & Gourine AV (2008). A role for TASK-1 (KCNK3) channels in the chemosensory control of breathing. *J Neurosci* **28**, 8844–8850.

Trapp S, Tucker SJ & Gourine AV (2011). Respiratory responses to hypercapnia and hypoxia in mice with genetic ablation of Kir5.1 (Kcnj16). *Exp Physiol* **96**, 451–459.

Waldmann R, Champigny G, Bassilana F, Heurteaux C & Lazdunski M (1997). A proton-gated cation channel involved in acid-sensing. *Nature* **386**, 173–177.

Wemmie JA, Price MP & Welsh MJ (2006). Acid-sensing ion channels: advances, questions and therapeutic opportunities. *Trends Neurosci* **29**, 578–586.

Weng JY, Lin YC & Lien CC (2010). Cell type-specific expression of acid-sensing ion channels in hippocampal interneurons. *J Neurosci* **30**, 6548–6558.

Xu F, Zhang Z & Frazier DT (2001). Microinjection of acetazolamide into the fastigial nucleus augments respiratory output in the rat. *J Appl Physiol* **91**, 2342–2350.

Ziemann AE, Allen JE, Dahdaleh NS, Drebot II, Coryell MW, Wunsch AM, Lynch CM, Faraci FM, Howard MA 3rd, Welsh MJ & Wemmie JA (2009). The amygdala is a chemosensor that detects carbon dioxide and acidosis to elicit fear behavior. *Cell* **139**, 1012–1021.

Author contributions

R.H.: *in vitro* recordings and experiments design, data analysis and interpretation, drafting the MS. S.L.P.M.: RT-PCR measurements, primer design, data interpretation, drafting the MS. Z.C.: *in vivo* recordings, drafting the MS; G.F.A.: *in vivo* recordings, experimental design, drafting the MS. D.R.M.: experimental design, *in vivo* recordings, data analysis and interpretation, drafting the MS. M.M.: project conception, experimental design, data analysis and interpretation, drafting the MS.

Acknowledgements

We are thankful for the outstanding technical assistance provided by Ms Weijie Jiang. This work was supported by NHLBI grants HL095731 (M.M.) and HL088580 (D.R.M.); R.H. was partly supported by NIH grant F31NS076201.